UCLA
UCLA Previously Published Works

Title

Dehydrogenation mechanisms of methyl-cyclohexane on γ-Al2O3 supported Pt13: Impact of cluster ductility

Permalink

Authors

Zhao, Wei
Chizallet, Céline
Sautet, Philippe
et al.

Publication Date

DOI

Supplemental Material

Dehydrogenation Mechanisms of Methyl-cyclohexane on $\gamma-Al_2O_3$ Supported Pt_{13}: Impact of Cluster Ductility

Wei Zhao,[1,2] Céline Chizallet,[1] Philippe Sautet,[2,3] Pascal Raybaud[1,]*

[1] IFP Energies nouvelles,

Rond-point de l'échangeur de Solaize, BP 3 - 69360 Solaize, France

[2] Université de Lyon, CNRS, Laboratoire de Chimie, Ecole Normale Supérieure de Lyon, 46 allée d'Italie, 69364 Lyon cedex 07, France

[3] Chemical and Biomolecular Engineering department, Chemistry and Biochemistry department and CNSI, University of California Los Angeles

Emails: christophezhao628@gmail.com, celine.chizallet@ifpen.fr,

sautet@ucla.edu , pascal.raybaud@ifpen.fr

* Corresponding author: Pascal Raybaud, email : pascal.raybaud@ifpen.fr , phone: +33.4.37.70.23.20, fax: +33.4.37.70.20.66

ABSTRACT

By using density functional theory (DFT) and ab initio molecular dynamics, we investigate the dehydrogenation reactivity of 13 atoms platinum cluster supported on the γ−alumina (100) surface. We provide a detailed free energy profile and structural analysis of the dehydrogenation mechanisms of methyl-cyclohexane (MCH) into toluene. We highlight the quantitative impact of dispersion corrections on the free energy profile and on the adsorption configurations of the intermediates exhibiting a dual interaction with the cluster and with the alumina surface. During the step by step dehydrogenation of MCH, several reconstructions of the Pt cluster and hydrogen migrations occur. Due to the cluster ductility, they are moderately activated and provide optimal active sites catalyzing the C-H bond cleavages. According to a preliminary kinetic analysis based either on energetic spans or on activation free energies of elementary steps, we found that many states and/or steps may be considered as determining ones. This may explain some diverging interpretations brought by previous experimental kinetic studies. We finally discuss how the cluster ductility challenges the historical concept of structure sensitivity/insensitivity for a given reaction in the case of nanometer-size metallic clusters dispersed on a support.

2

1. INTRODUCTION

Metallic active phases in a highly dispersed state on oxide supports represent an important class of heterogeneous catalyst involved in many chemical processes. However, understanding and tuning the structural, electronic and catalytic properties of supported metallic clusters with sub-nanometric sizes, remains challenging for experimental characterization, even when using high resolution and/or operando/in situ techniques.[1-4] In particular, the level of complexity of these systems rises due to the ductility of the metallic nano-clusters or in other words, their reconstruction induced by their environment (temperature, pressure, support, adsorbed intermediates…) as it has been highlighted by previous theoretical[5-11] and experimental studies.[1-3, 12] It can be underlined that such a ductility is sometimes called "fluxionality",[11] although the latter more precisely refers to a process that in the end does not change the structure of the considered compound, as originally defined by Cotton.[13]

Among others, platinum based nano-clusters supported on γ–alumina (γ-Al$_2$O$_3$) are well known to be active catalysts in naphtha reforming catalytic processes,[14] and light alkane non-oxidative dehydrogenation.[15, 16] Catalytic reforming is one important process in the refining industry aiming at the transformation of petroleum fractions (naphtha) with a low research octane number into a high octane reformate through dehydrogenation and cyclisation reactions.[17-19] Regarding dehydrogenation, there is still an open question whether dehydrogenation of hydrocarbons (HCs) catalyzed by platinum is a "structure sensitive" or "structure insensitive" reaction according to the original Boudart's definition which predominantly focuses on size effect.[20] Historically, it was reported that cycloalkane dehydrogenation should be size insensitive,[20-24] whereas more recent studies underlined the role of the local structure and coordination of sites in dehydrogenation of alkanes.[16, 22,

23, 25-29] As we will discuss it in this work, answering this question needs to take into account the afore-mentioned structural ductility of the platinum nano-clusters.

In any cases, high activity towards the targeted dehydrogenation and dehydrocyclization reactions, while avoiding undesired reactions as hydrogenolysis and coking, requires only small amounts of platinum. The industrial reforming catalysts usually contain 0.2-0.4 wt% of platinum supported on alumina and the corresponding size of the platinum nanoparticles is close to 1 nanometer (thus containing between 10 and 20 atoms) with a very high dispersion close to 100%.[22, 23, 30-33] A second metallic element such as rhenium[34-38] or tin[31, 32, 39-42] is often added to improve the selectivity to aromatics and reduce deactivation of catalysts by coke formation.[34, 39, 40, 43, 44] The superior activity of platinum for C-H bond scission and low activity for C-C bond cleavage also made the γ–alumina supported platinum catalyst as a popular choice for the non-oxidative dehydrogenation of light olefins.[15] In the case of reforming, γ–alumina is the most suitable support enabling the good dispersion of Pt clusters and catalyzing cyclisation and isomerization reactions, through the possible addition of a chlorine dopant modulating the acidity of the support.[18, 22, 45, 46]

Due to the high level of complexity inherent to the reaction networks involved in naphtha reforming, model reactions have to be chosen for a better understanding of the catalytic properties.[47-52] A very popular one is the reforming of n-heptane, which already give rise to many reaction pathways, such as dehydrogenation, dehydrocyclization but also isomerization, cracking, hydrogenolysis and coking that may concomitantly occur.[17, 22, 48] In this work, we will focus on the mechanism of a more simple but essential model reaction: dehydrogenation of methyl-cyclohexane (MCH) to toluene. This reaction aims at probing predominantly the catalytic properties of the metallic nano-clusters with respect to their dehydrogenation ability, in the absence of any secondary reactions. It has also been the

subject of numerous experimental kinetic investigations on mono- or bi-metallic platinum based catalysts,[26, 35, 52-60] sometimes combined with kinetic modeling.[35, 54-57] However, many questions remain open about the relevant mechanisms, rate determining step and corresponding kinetic parameters. In particular, there is a wide range of reported experimental apparent activation energies varying from 15 kJ/mol up to 220 kJ/mol depending on several hypotheses: the physico-chemical properties of the catalysts (platinum loading, dispersion, sizes…), the reaction conditions (temperature, pressure, space time…) and the kinetic model used (power rate law or more refined Langmuir-Hinshelwood-Hougen-Watson (LHHW) rate equations).[28, 35, 53, 55, 56, 61, 62] It is thus the purpose of the present theoretical approach to provide atomic scale insights into the elementary steps and to determine more quantitative intrinsic kinetic parameters in order to help for the improvement of the experimental interpretation.

Recent progresses in density functional theory (DFT) calculations have allowed researchers to investigate more and more complex catalytic systems[63] and in particular, the structural, electronic and reactive properties of alumina supported platinum nano-clusters containing up to 13 atoms [1, 6-8, 64] which are close to industrial systems used in reforming process or alkane dehydrogenation reactions. This methodology is also commonly applied to the identification of key intermediates and transition states, on extended metallic surfaces, involved in the activation of C-H and C-C bonds at the core of hydrogenation/dehydrogenation and hydrogenolysis reactions. Hence, ideal Pt(111) surfaces have been extensively used for the modeling of the hydrogenation/dehydrogenation reaction of small alkene/alkane molecules (ethylene or propene)[16, 65-70] and aromatics/cycloalkanes.[71-78] Regarding the mechanisms of benzene hydrogenation, Morin et al.[73] found that the reaction passes through surface intermediates: monohydrobenzene $\rightarrow$ dihydro-1,3-benzene $\rightarrow$ trihydro-1,3,5-benzene. Saeys et al.[74, 75] studied an alternative

pathway, competitive with the previous one, involving cyclohexadiene and cyclohexene as intermediates. Sabbe et al.[77] proposed an *ab initio* micro-kinetic simulation based on periodic DFT calculations for the full network of benzene hydrogenation on Pt(111) and found the following pathway to be dominant: monohydrobenzene → 1,3-cyclohexadiene (or dihydro-1,2-benzene) → trihydro-1,2,3-benzene → cyclohexene (or tetrahydro-1,2,3,4-benzene).

However, the reverse reaction (dehydrogenation) involving the less symmetric methyl-cyclohexane and toluene molecules was more rarely studied, even on extended surface. One of the unique theoretical work on toluene hydrogenation reaction on Pt(111) proposes a *first-principles* kinetic model using DFT calculations achieved on benzene hydrogenation.[75] To the best of our knowledge, the simulation of methyl-cyclohexane dehydrogenation on a γ−alumina supported platinum cluster (representative of reforming catalyst) remains so far unexplored in the literature. As mentioned before, some of our previous DFT studies showed that the morphology and local structure of Pt_{13} clusters are affected either by the underlying γ-alumina support,[5-7, 64] by the hydrogen pressure,[1, 7] and also by the nature of intermediates involved in C-H and C-C bond breakings of ethane.[8] The morphology and electronic properties of the platinum cluster were also shown to be very sensitive to the hydrogen pressure such as applied in the reforming conditions.[1, 7] By increasing the hydrogen coverage on the surface of these nano-particles, a reconstruction takes place, from the bi-planar (BP) structure at low hydrogen coverage to a cuboctahedron one at H/Pt ratio higher than 1.5. This structural reconstruction due to the cluster ductility is associated with a large change of the electronic properties of the platinum sites, from a metallic to a partially oxidized state. This phenomenon has been confirmed experimentally by X-ray absorption spectroscopy: XANES revealed that the hydrogen coverage at 25°C increases from ~1.9 to

~2.5 H/Pt when the H_2 pressure increases from 10^{-5} to 1 bar,[1] while EXAFS revealed a shape change from two-dimensional to three dimensional at even higher H_2 pressure.[2]

Further understanding of the atomic scale behavior of Pt clusters in model reactions, and simultaneously elucidating the reaction mechanisms by DFT methods, will have significant implications for the improvement of such complex heterogeneous catalysts. This is particularly true for MCH dehydrogenation catalyzed by supported platinum nano-particles in order to better control the reactivity and selectivity of naphtha reforming catalysts as a function of temperature, and $P(H_2)/P(HC)$ pressure ratio.[50]

In this work, using previously developed models of Pt_{13} cluster supported on γ-Al_2O_3 particles,[1, 6, 7, 63] we will determine the free energy profiles of the dehydrogenation of MCH in toluene by DFT calculations. Due to the complexity of the reaction network, we will first identify one representative dehydrogenation pathway involving 4-methylcyclohexene based on a preliminary analysis of the stability of various unsaturated intermediates as a function of Pt sites, by combining static and molecular dynamics approaches. The complete Gibbs free energy profiles will then be established at the PBE-dDsC level for two relevant experimental temperatures (625 K and 800 K) and the various elementary steps involved will be analyzed in details. In the course of manuscript, we will analyze the effect of dispersion corrections in the DFT functional. Finally, we will show how these results shed new light on the structure sensitivity concept of the MCH dehydrogenation reaction.

2. METHODS

2.1 Atomistic model of the catalyst

We consider here the dehydrated and non-chlorinated (100) $\gamma-$alumina surface as determined in previous works[46, 79, 80] by using the bulk model of $\gamma-$alumina proposed by Krokidis et al.[81] On this facet, the alumina support stabilizes a Pt_{13} cluster with a BP structure interacting with the $\gamma-$alumina surface through 7 platinum atoms (S1 to S7 in **Figure 1**). [6, 7, 64]

According to previous DFT results,[7] under catalytic reforming conditions (temperature of 800 K and a hydrogen partial pressure close to 10 bar), an interval of 6 to 18 hydrogen atoms per cluster corresponds to the most stable configurations. When compared to *in situ* XANES experiments,[1, 2] H/Pt values closer to the lowest limit (6-8) of this interval was found to be relevant in similar (T, P) conditions. In addition, considering the bulkiness of the methyl-cyclohexane reactant and toluene product, the accessibility of both molecules to metal sites as well as the C-H bond scission would be strongly hindered for the highest number of H (>13). So, we decided to undertake the present study with 6 hydrogen atoms covering the Pt_{13} cluster (**Figure 1**), which corresponds to the lowest limit.

In this case, the BP morphology of the cluster is only slightly modified with respect to the bare cluster. This allows us to define the Pt layer interacting with the alumina surface (7 atoms labelled with letter "S"), and the layer contacting with vacuum (6 atoms with letter "V"). Likewise, we define all the hydrogen atoms by using the "Hi" terminology, i being the number of the platinum atom on which the H is adsorbed. We will start our mechanistic investigations by considering all those different adsorption sites, with migration of hydrogen atoms on the metal particles when needed.
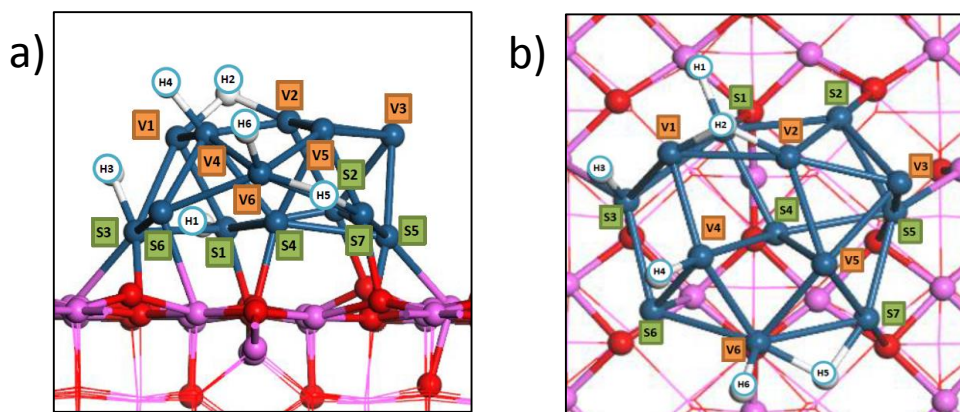
Figure 1. Molecular structure of the starting model of Pt$_{13}$/γ-Al$_2$O$_3$ (100) with 6 adsorbed hydrogen atoms. a) side view, b) top view. Pt atoms labelled with letter "S" are located at the alumina surface, Pt atoms labelled with letter "V" are in contact with vacuum. Color legend: aluminum (pink balls), oxygen (red balls), platinum (dark blue balls), hydrogen (white balls)

The Pt$_{13}$/γ-Al$_2$O$_3$ (100) system considered in the present study consists of a 3D-periodic cell, the size of which is $16.7 \times 16.8 \times 25.8$ Å^3, occupied by a γ-Al$_2$O$_3$ slab whose thickness is 7.2 Å (with its surface perpendicular to the z axis). Each slab is periodically separated by a vacuum layer of 18.6 Å. Free gas phase molecules were simulated within $25 \times 25 \times 25$ Å^3 cells for all C$_7$ molecules, and a $20 \times 20 \times 20$ Å^3 cell for H$_2$ in order to prevent lateral interactions between replicas.

2.2 Total energy calculations

All calculations were performed by using the periodic plane-wave DFT formalism as implemented in the VASP Package (versions 5.3.5 and 5.4.1, with careful checks of consistency between the two versions).[82, 83] The PBE[84] and PBE-dDsC[85, 86] functionals were applied. In PBE-dDsC, the atom pair specific parameters (dispersion coefficients and short-range damping strength) are determined from the electron density. Thus, PBE-dDsC accounts for van der Waals (vdW) dispersion forces, which may impact molecular adsorption on surface. Our preferential choice for this functional was guided by the

systematic benchmark by S. Gautier et al.[87], showing that PBE-dDsC is one of the best compromise for predicting adsorption energies of aromatics and unsaturated HCs on Pt(111).

In practice, all geometries were optimized and all energies were determined at both PBE and PBE-dDsC levels. The vibrational analysis required for the estimation of enthalpies and entropies was generally performed at the PBE level, except when significant geometry discrepancies were observed between the configurations optimized by using the two functionals (as it will be commented in the text).

The projected augmented wave (PAW) method[88, 89] was used to describe the core-electron interactions and the electron wave functions are developed on a set of plane waves with a cut-off energy of 400 eV. The electronic convergence criterion was 10^{-6} eV.

2.3 Identification of local energy minima

2.3.1 Static geometry optimization

The convergence criterion on forces for nuclei was 0.01 eV/Å for geometry optimizations. Only the two uppermost alumina layers, the platinum cluster and the adsorbed molecule were allowed to relax.

To check the sensitivity of the stability to the adsorption sites, different possible adsorption sites (20) have been carefully tested (**supporting information 1**) as a function of the molecule orientation in the case of 4-MCHe, known as a key reaction intermediate.[35, 53-56, 90-93] After considering 57 different conformations, 4-MCHe adsorbed on the V3 site (**Figure 1**) in the π mode was found to be the most stable adsorption. Thus, this V3 site will be used as the most relevant one for the whole reaction pathway. We also noticed that for this given adsorption site (V3) and π mode, several local energy minima of the system are found according to the orientation of 4-MCHe. The impact of the conformation on energy on the V3 site is discussed in **supporting information 2.** Since the energy variation remains within an

interval of 16 kJ/mol as a function of rotated configurations, this implies that temperature effect (at 625 K or 800 K in experimental conditions) may allow the molecule to explore various metastable states on this given site. Thus, complementary ab initio molecular dynamics (AIMD) simulations were undertaken to explore possible thermal effects on all structures.

2.3.2 *Ab initio* molecular dynamics

We applied velocity scaled *ab initio* molecular dynamics (AIMD) at the PBE level, in order to overcome the lowest energy barriers and explore different possible structures for the supported Pt_{13} cluster and the corresponding conformations of adsorbates. A time step of 5 fs was chosen and the hydrogen mass was fixed at 10 g/mol instead of 1 g/mol to accelerate the exploration of the potential energy surface. Three distinct temperatures of 500 K, 800 K and 1200 K were employed in order to speed up the migration of atoms and the number of explored configurations. The same set of atoms as during geometry optimization (see above) was kept fixed during AIMD. For the selected low energy configurations identified during AIMD, subsequent "quenching" steps of geometry optimization at 0 K were applied in order to obtain well-defined energies at the PBE and PBE-dDsC levels. This approach is described in details for the 4-MCHe intermediate in **supporting information 3.**
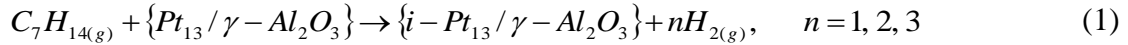
2.4 Transition states search

To identify saddle points and minimum energy paths between two stable intermediates being local minima on the potential energy surface, we mainly used the nudged elastic band (NEB) method.[94, 95] The initial path was built through an interpolation scheme involving both cartesian and internal coordinates according to the Opt'n-Path algorithm.[96] We first used the NEB algorithm between the initial and final states, as implemented in the VASP

Transition State Theory (VTST) module,[97] then picked up the points near the higher energy point among the results and performed a climbing-image NEB (CI-NEB) calculation.[98] The new higher energy point is then relaxed using a quasi-Newton algorithm[99] until convergence criteria are reached (forces on ions smaller than 0.01 eV·Å^{-1}).

2.5 Gibbs free energy profiles for the dehydrogenation of MCH into toluene

The MCH dehydrogenation reaction from the gas phase to an adsorbed intermediate i and the simultaneous release of gas phase dihydrogen (**Equation (1)**) was quantified by the Gibbs free energy of dehydrogenation, $\Delta_r G_{dehyd,MCH(g)}$, as defined by **Equation (2)**:

$$C_7H_{14(g)} + \{Pt_{13}/\gamma - Al_2O_3\} \rightarrow \{i - Pt_{13}/\gamma - Al_2O_3\} + nH_{2(g)}, \quad n = 1, 2, 3 \qquad (1)$$

where $i = C_7H_{14-2n}$,

$$\Delta_r G_{dehyd,MCH_{(g)}}(i) = G_i + nG_{H_{2(g)}} - G_{MCH_{(g)}} - G_{Pt_{13}/\gamma - Al_2O_3}, \quad n = 1, 2, 3 \qquad (2)$$

Electronic energy, enthalpy and entropy terms of the same dehydrogenation reaction were defined similarly as $\Delta_r E_{dehyd,MCH_{(g)}}$, $\Delta_r H_{dehyd,MCH_{(g)}}$ and $T\Delta_r S_{dehyd,MCH_{(g)}}$, respectively.

For the study and analysis of the Gibbs free energy profile of the dehydrogenation reaction, we considered the successive mono-dehydrogenation of MCH into toluene (6 successive C-H cleavages) involving the formation of partially dehydrogenated intermediates with H atoms co-adsorbed on the Pt cluster. At each step, one extra hydrogen is thus transferred from the molecule to the cluster. Once two successive H atoms are dissociated from the molecule on the cluster, one H$_2$ molecule is desorbed in gas phase so that the number of H atoms adsorbed on the clusters is comprised between 6 and 8 along the reaction pathway. For the analysis of each elementary step, we calculated the energy, enthalpy, entropy terms, and Gibbs free energy of reaction and activation corresponding to the transformation of

intermediate i to the subsequent intermediate via transition state (TS_i): the same energy components ($X=E, H, TS$) are noted $\Delta_r X_{i \to TS_i}$ and $\Delta_r X^{\ddagger}_{i \to TS_i}$, respectively.

The vibrational frequencies and the partition functions to deduce enthalpy, entropy and Gibbs free energies were calculated according to the methodology described in details in **supporting information 4 and 5**. These thermodynamic data were evaluated for two relevant temperatures (625 K and 800 K), and at 1 bar pressure.

3. RESULTS

3.1 Preliminary analysis of the stability of the intermediates involved in MCH dehydrogenation

If one analyzes the complete reaction network by considering all possible mono-dehydrogenation steps, more than 40 possible surface intermediates may be formed during the subsequent C-H bond breaking steps. In addition, for each intermediate, several adsorption configurations on the platinum cluster may exist which implies that an exhaustive investigation cannot be handled by DFT simulations. Nevertheless, in numerous studies, the proposed mechanism for the dehydrogenation of methyl-cyclohexane (MCH) into toluene (Tol) involves two key intermediates:[35, 53-56, 90-93] methyl-cyclohexene (MCHe) and methyl-cyclohexadiene (MCHde). The study of the relative stabilities of the C_7H_{12} intermediates (including MCHe and 6 related isomers) adsorbed on $Pt_{13}H_6/\gamma-Al_2O_3(100)$ showed that radical type intermediates are far less stable than the conjugated methyl-cyclohexene adsorbed through π bonding (**supporting information 6**). In particular, 4-methyl-cyclohexene (4-MCHe) and 1-MCHe are the two most stable intermediates. Since we suspect that the close vicinity of the methyl-group with the two C-H bonds to be broken will make more difficult the C-H bond cleavage, 4-MCHe on $Pt_{13}H_6/\gamma-Al_2O_3$ was chosen as the

relevant intermediate of methyl-cyclohexane dehydrogenation to be used as a benchmark for the reaction network.

Thus, we decided to focus on the 10 relevant intermediates invoked in the literature and considered the simplified reaction network of MCH dehydrogenation into toluene illustrated in **Figure 2**. The 6 successive C-H cleavage steps produce 3 radical intermediates: methyl-cyclohexyl (C_7H_{13}), methyl-cyclohexenyl (C_7H_{11}), and methyl-cyclohexadienyl (C_7H_9).
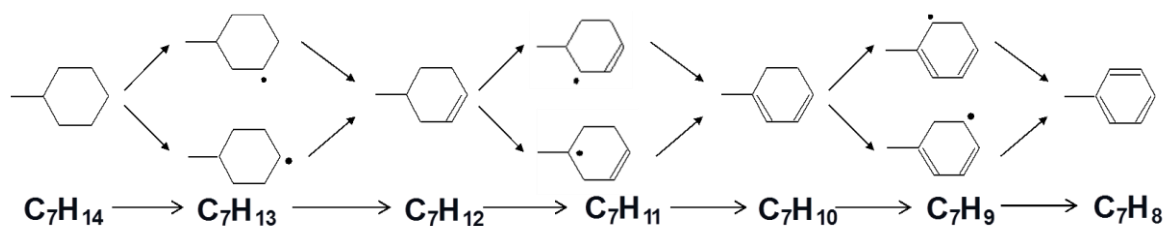

Figure 2. Simplified network for the dehydrogenation of MCH into toluene via 4-methyl-cyclohexene (4-MCHe) and methyl-cyclohexadiene (MCHde) intermediates.

Moreover considering the PBE energy profile for these 6 mono-dehydrogenation steps of MCH into toluene (**Supporting information 7),** the lowest energy pathway involves the C_7H_{13}, C_7H_{11} and C_7H_9 intermediates represented at the bottom of the network of **Figure 2**. However, since it was not possible to identify a transition state connecting C_7H_{12} and the most stable C_7H_{11} intermediate, we consider the pathway involving the second radical C_7H_{11} intermediate in what follows.

3.2 Mechanisms and free energy profiles of methyl-cyclohexane dehydrogenation

According to the previous analysis, we will calculate electronic energy, enthalpy, entropy and Gibbs free energy for each intermediate and transition state involved in the simplified reaction sequence illustrated in **Figure 3.**

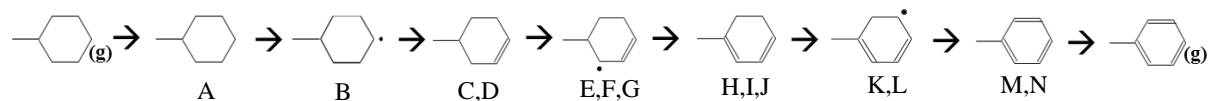(g) → A → B → C,D → E,F,G → H,I,J → K,L → M,N → (g)

Figure 3. Sequence of intermediates simulated for the dehydrogenation of MCH into toluene investigated in the present study. The corresponding names of intermediates and the meaning of each letter are given in Table 1.

We recall that according to the dedicated study on 4-MCHe (**supporting information 3**), we included systematically AIMD simulations to take into account the ductility effect of the clusters and determine the optimal conformations, as a function of the adsorbed intermediate. We also explored if a cluster geometry found for another adsorbed intermediate can be valid also for the given intermediate, thus by crossing the morphology-adsorbate couples.

In what follows, we will present predominantly the results obtained with PBE-dDsC functional in order to include dispersion corrections. When required, we will discuss in more details the differences between PBE vs PBE-dDsC.

We will discuss first the temperature of 625 K, since this temperature is generally the one or close to the one used in MCH dehydrogenation kinetic experiments.[35, 55, 56, 61] In addition, since the naphtha reforming process is generally performed at a higher temperature, we will also report DFT results calculated at 800 K, which will allow us to highlight the sensitivity of our model with respect to the reaction conditions.

3.2.1 General trend and temperature effect

Table 1 reports the elementary steps and associated intermediates identified along the reaction pathway, including the expected the 6 C-H bond cleavages, MCH adsorption, Toluene desorption and 3 H_2 desorption steps. Cluster reconstruction and diffusion steps of H

atoms on the cluster are also included. Moreover, the number of hydrogen atoms on the cluster fluctuates according to the sequence 6→7→8→6, H_2 desorption sequentially occurring after two C-H bond cleavage steps.

Table 1. Various intermediates and nature of elementary steps along the dehydrogenation of methyl-cyclohexane on $Pt_{13}H_6/Al_2O_3$ (100)

Surface intermediates		Elementary step		TS	Reaction type
ref	Methyl-cyclohexane (gas)	--		--	--
(A)	Methyl-cyclohexane	(1)	MCH (g) → A	--	MCH adsorption
(B)	Methyl-cyclohexyl + H	(2)	A → B	TS_a	C-H bond cleavage
(C)	Methyl-cyclohexene + 2H	(3)	B → C	TS_b	C-H bond cleavage
(D)	Methyl-cyclohexene	(4)	C → D + H_2	--	H_2 desorption
(E)	Methyl-cyclohexenyl + H	(5)	D → E	TS_d	C-H bond cleavage
(F)	Methyl-cyclohexenyl + H	(6)	E → F	TS_e	H atom migration
(G)	Methyl-cyclohexenyl + H	(7)	F → G	TS_f	cluster reconstruction
(H)	Methyl-cyclohexadiene + 2H	(8)	G → H	TS_g	C-H bond cleavage
(I)	Methyl-cyclohexadiene	(9)	H → I + H_2	--	H_2 desorption
(J)	Methyl-cyclohexadiene	(10)	I → J	TS_i	cluster reconstruction
(K)	Methyl-cyclohexadienyl + H	(11)	J → K	TS_j	C-H bond cleavage
(L)	Methyl-cyclohexadienyl + H	(12)	K → L	TS_k	H atom migration
(M)	Toluene + 2H	(13)	L → M	TS_l	C-H bond cleavage
(N)	Toluene	(14)	M → N + H_2	--	H_2 desorption
	Toluene (gas phase)	(15)	N → Tol (g)	--	toluene desorption

The electronic energy profile at 0 K and the free energy profiles (including transition states) at 625 K and 800 K are illustrated in **Figure 4** where the three (cluster+6H)

morphologies are represented with different colors, along with the original cluster stable only at the beginning and end of the catalytic cycle (grey). The numerical data corresponding to **Figure 4** are given in **supporting information 8,** together with the results obtained with the PBE functional. The experimental thermodynamic of the overall gas phase reaction (MCH→Toluene+3H$_2$) is well reproduced by the theoretical thermodynamic (particularly at the PBE-dDsC level). At 625 K, the experimental reaction enthalpy,[100] $\Delta_r H_{dehyd,MCH_{(g)}}(Tol)$, and $\Delta_r G_{dehyd,MCH_{(g)}}(Tol)$ are equal to 216 kJ/mol and -32 kJ/mol respectively, while the calculated values are 219 and -42 kJ/mol respectively.

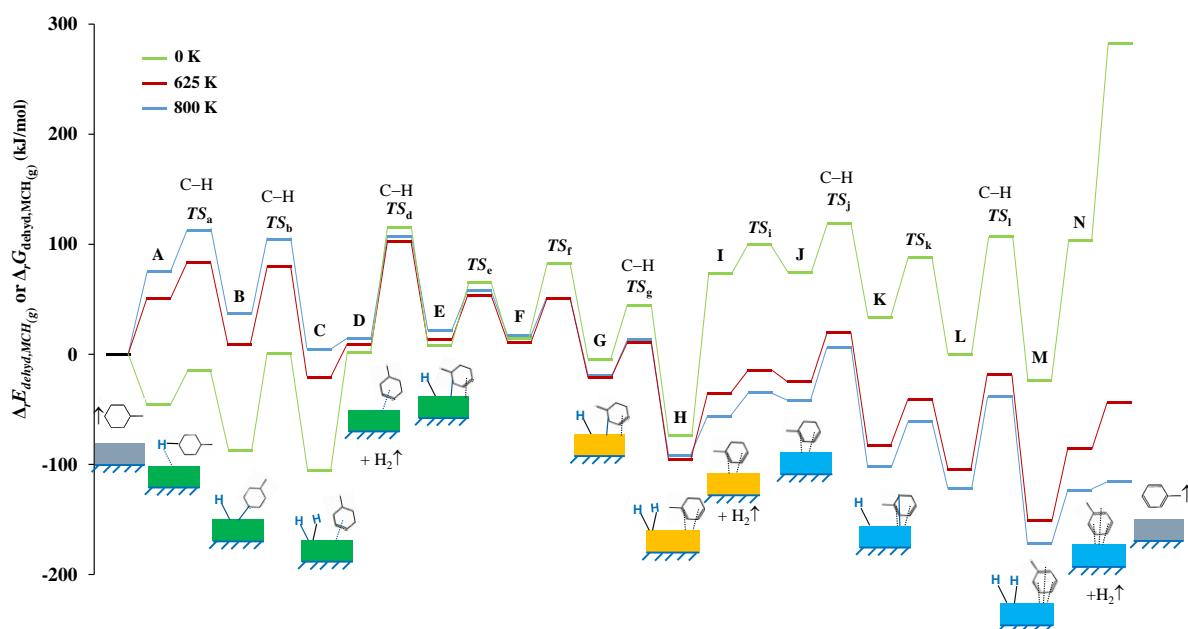**Figure 4. Free energy profile (PBE-dDsC level) for methyl-cyclohexane dehydrogenation over Pt$_{13}$H$_6$/γ-Al$_2$O$_3$ at 0 K, 625 K and 800 K. Each colored box represents the cluster with 6 H atoms and various colors correspond to different cluster morphologies (also highlighted in Figures 5 and 6 with the same color coding).**

The expected effect of temperature is clearly recovered for this endothermic reaction: the higher the temperature, the more exergonic the reaction. Nevertheless, a closer analysis of the profile reveals actually two different effects of temperature along the reaction pathway. Before the formation of methyl-cyclohexenyl+H (F), the temperature increase destabilizes all

intermediates, whereas beyond (F), the profile becomes more exergonic. Thus a crossing point in Gibbs free energy is observed around intermediate (F). This trend is not related to the enthalpy terms, which variation is rather modest particularly for the two highest temperatures (**Table S6**). By contrast, it is mainly driven by the entropy term (TΔS). Hence, before the formation of intermediate (F), the cumulative entropic terms are negative, whereas they become positive after (F). As H_2 molecules are formed and released in gas phase sequentially, the entropy of the system increases. Notably, this effect becomes significant after the formation of methyl-cyclohexadiene (I) associated to the desorption of the second H_2 molecules (step H$\rightarrow$I). This trend is significantly enhanced after the desorption of the third H_2 molecule (M$\rightarrow$N) and of toluene. In particular, the Gibbs free energy of this desorption step decreases from 0 K to 800 K by about 170 kJ/mol. This observation qualitatively explains why the usual experimental conditions chosen for MCH dehydrogenation and for the industrial reforming process employs preferentially high temperatures (625 K and 800 K, respectively), not only because the overall reaction is endothermic, but also because toluene desorption is favored at high temperatures. By contrast, temperature increase disfavors the MCH adsorption step for the same entropic reasons. Temperature has much weaker effects (although not totally negligible) on the other elementary steps that do not involve adsorption or desorption : C-H bond cleavage, cluster reconstruction and H atom migration steps (which involve only vibrational entropy changes).

The Gibbs free energy profiles at 625 K calculated with PBE-dDsC and PBE are compared in **Figure S8**. Apart from the first methyl-cyclohexane adsorption step and the last toluene desorption step, the PBE-dDsC free energy profile is shifted to lower energy levels by about 30 kJ/mol with respect to the PBE profile, while this shift is 60 kJ/mol for methyl-cyclohexane (A) and 40 kJ/mol for methyl-cyclohexyl (B). For all intermediates and

18

transition states with the exception of A➔B➔C steps (see further explanations), the structures almost do not depend on the functional.

In what follows, we will analyze all the elementary steps and their key energy components according to the 5 families of reactions described in **Table 1**: methyl-cyclohexane adsorption and toluene desorption, C-H bond cleavages, cluster reconstructions, H atom migrations, H_2 desorption.

3.2.2 Adsorption, desorption and diffusion steps

- **Methyl-cyclohexane adsorption**

The methyl-cyclohexane adsorption occurs through a physisorption step, which is a precursor state before the first C-H bond cleavage. It is important to underline that the adsorption mode is a flat one where the molecule is located predominantly on the alumina surface in the close vicinity of the Pt cluster (**Figure 5 b**). This flat configuration is particularly favorable with the PBE-dDsC functional, whereas with PBE functional an alternative perpendicular configuration may compete (**Figure 5 a**). The PBE-dDsC adsorption energy of methyl-cyclohexane in a parallel orientation to the alumina is more exothermic (-45 kJ/mol) than in a perpendicular position (1 kJ/mol) due to dispersion effects. By contrast, with the PBE functional, both configurations of methyl-cyclohexane are rather close in energy: +21 kJ/mol in a perpendicular mode and +17 kJ/mol in the parallel one. As a consequence, the adsorption energy with PBE-dDsC is thus more stable by 62 kJ/mol. As we will discussed it later, this will also impact the subsequent steps (A→B→C). At T=625 K, this adsorption step is exothermic ($\Delta_r H$ = -40 kJ/mol, see **Table S8**) and endergonic ($\Delta_r G$ = 51 kJ/mol). The large difference between enthalpy and free energy is due to the loss of rotational and translational entropies partially compensated by vibrational entropy during this physisorption step. Indeed, in gas phase, the TS_{vib} and $T(S_{rot} + S_{trans})$ terms are equal to 115 and 191 kJ/mol,

respectively, which means that the loss of rotational and translational entropies (assuming adsorbed MCH as an immobile complex) is thus counterbalanced by a non-negligible contribution of the vibrational entropic term recovered in the adsorbed state and accounting for 215 kJ/mol. In any case, the entropy loss is mainly at the origin of the positive Gibbs free energy and causes a free energy barrier for the process.
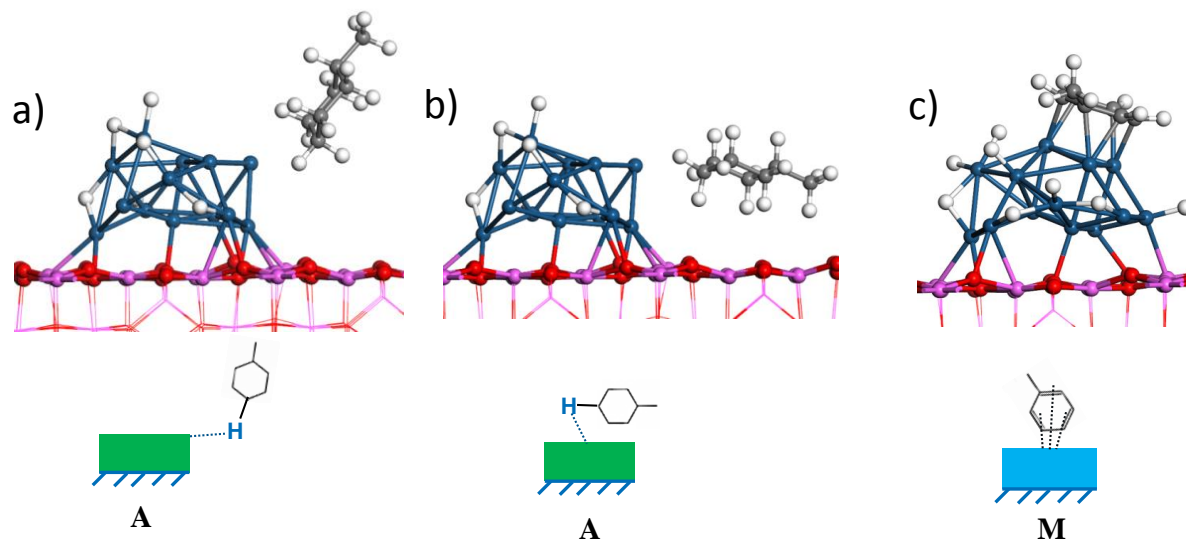

Figure 5. Adsorption of (A) methyl-cyclohexane a) in the perpendicular mode, b) in the flat mode, and c) of (M) toluene on $Pt_{13}H_6$/γ-Al_2O_3. Color legend: aluminum (pink balls), oxygen (red balls), platinum (dark blue balls), carbon (dark grey balls), hydrogen (white balls)

- **Toluene desorption**

By contrast, at T=625K the toluene desorption step is highly endothermic ($\Delta_r H$=+174 kJ/mol) and endergonic due to a large gain of entropy (T$\Delta_r S$=+130 kJ/mol, see **Table S8**) due to the release of toluene from the adsorbed state to gas phase. The gas phase TS_{vib} and T(S_{rot}+ S_{trans}) terms are equal to 93 and 189 kJ/mol, respectively, thus slightly lower than for MCH. Nevertheless, the vibrational entropic term in the adsorbed state (TS_{vib}=152 kJ/mol) is lower than the one previously reported for MCH which implies that the resulting entropy variation is larger than the one of MCH.

The free energy variation of this step is hence strongly temperature dependent (**Figure 4**): the higher the temperature, the lower the Gibbs free energy barrier for toluene desorption. Notably, the 3 fold hollow type of toluene adsorption mode strongly impacts the shape of the cluster with respect to the starting structure. **Figure 5 c)** illustrates again the cluster ductility by showing how the toluene pulls out the 3 adsorption sites (V2-V3-V5) which significantly distorts the initial bilayer structure. Previous DFT calculations [71, 73, 78, 101] found slightly different adsorption modes for benzene on Pt (111) surface, which highlights the specific cluster's behavior.

- **Hydrogen desorption and diffusion**

As explained before, the number of hydrogen atoms on the cluster fluctuates as $6 \rightarrow 7 \rightarrow 8 \rightarrow 6$ along the reaction pathway. Hence, after two successive C-H bond cleavages, one H_2 molecule is desorbed in gas phase from the two H atoms transferred from the HC molecule. This choice is also consistent with the intuitive understanding that increasing hydrogen coverage of the cluster hinders dehydrogenation steps. The three H_2 molecule desorption steps are all endothermic and endergonic (**Figure 4** and **Table S9**), in spite of the significant gain of rotational and translational entropies ($T\Delta_r S$=59-81 kJ/mol at 625 K). Although these entropy terms are lower than those of toluene and MCH (130 and 91 kJ/mol, respectively), they are non-negligible. This can be explained by the weaker contribution of vibrational entropic terms of the 3 systems (C, H, M) with 2 adsorbed H atoms (TS_{vib}=23, 14 and 36 kJ/mol, respectively) which only modestly counterbalance the gas phase contribution by contrast with adsorbed toluene and MCH. Hence, the Gibbs free energy of these steps (comprised between 29 and 65 kJ/mol at 625 K) depends on the reaction temperature: the higher the temperature, the lower the barrier. As underlined by in situ XANES experiments combined with DFT calculations,[1] and by the comparison of functionals for adsorption on a

Pt(111) surface,[102] there are clear indications that the DFT/PBE calculations slightly overestimate the stability of H atoms adsorbed on the cluster.

The search of the transition state for the first H_2 desorption shows that the energy of the transition state is very close to the final state (**supporting information 9**). It also means that the backward reaction, i.e. the dissociative adsorption of H_2 molecule onto the cluster, is not activated. This result is consistent with previous ones reported on the Pt(111) surface, where the adsorption step of hydrogen is not activated.[103, 104] As a result, the activation free energies for the H_2 molecule desorption steps are considered identical to their reaction free energy.

Along the reaction pathway, including diffusion of H atoms on the cluster was also required in two cases: either to minimize steric hindrance preventing the forthcoming C-H bond scission due to instability of the dehydrogenated intermediates (such as K → L, **Figure S10**), or to Pt site occupancy (E → F, **Figure S10**). These elementary steps are both exergonic (**Table S10**) and their activation free energies are rather close (41-42 kJ/mol at 625 K). In all other cases, the C-H bond scissions can proceed without considering such a preliminary H diffusion.

3.2.3 Cluster structural changes

As pointed out in our previous theoretical studies,[6, 7] the reaction environment as well as the support induce morphology changes of the Pt_{13} cluster. In the present case, we find that four main cluster reconstructions occur and lead to three morphologies distinct from the initial structure along the dehydrogenation path (**Figure 6** and **Table S11**). These reconstructions are accompanied also by hydrogen migrations on the cluster. The deformed clusters obtained by AIMD stabilize the adsorbed intermediates in the course of dehydrogenation reaction, which reflects the ductility of the supported cluster.
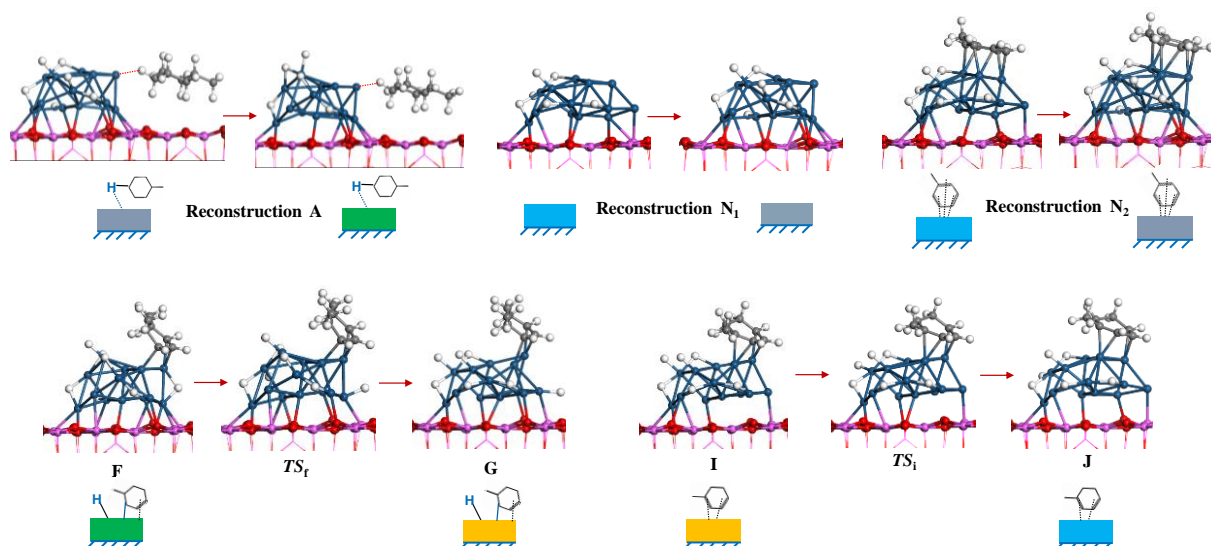
Figure 6. Molecular structures along the cluster reconstruction steps (PBE-dDsC level). Color legend: aluminum (pink balls), oxygen (red balls), platinum (dark blue balls), carbon (dark grey balls), hydrogen (white balls)

The initial cluster structure (with 6 H atoms adsorbed on it) does not remain as the most stable configuration when the reactant, methyl-cyclohexyl, methyl-cyclohexene and toluene are adsorbed on it. So, at the beginning of the reaction, the cluster slightly reconstructs before methyl-cyclohexyl is formed (green cluster in **Figure 6**). If we assume that methyl-cyclohexane is first adsorbed on the initial non-reconstructed cluster (grey), the corresponding electronic energy variation $\Delta_r E$ (reconstruction A in **Figure 6**) is +35 kJ/mol while the free energy variation $\Delta_r G$ is about +25 kJ/mol. If we assume that the reconstruction step occurs before methyl-cyclohexane adsorption (cluster reconstruction from grey to green without adsorbed molecule), the energy cost is very similar: $\Delta_r E$= +37 kJ/mol, which means that the methylcyclohexane physisorption does not impact strongly the cluster reconstruction. At the same time, the adsorption energies of methyl-cyclohexane ($\Delta_r E$= -82 before the reconstruction vs -80 kJ/mol after the reconstruction) does not depend strongly whether the cluster is reconstructed or not. So, the reconstruction might occur either before or after methylcyclohexane physisorption.

Regarding the last step, toluene is proved to be more stable on the deformed cluster (blue cluster in **Figure 6**) than on the initial cluster found by AIMD. Once toluene is desorbed from the blue cluster, there is actually a supplementary step to restore the morphology of the initial cluster (grey). From a thermodynamic point of view, toluene desorption exhibits an electronic energy $\Delta_r E$ of +220 kJ/mol, corresponding to $\Delta_r G$ of +89 kJ/mol, while the subsequent cluster reconstruction involves $\Delta_r E$= -41 kJ/mol and $\Delta_r G$= -25 kJ/mol (Reconstruction N_1). If one assumes that the reconstruction occurs first in presence of adsorbed toluene and then the desorption occurs, the energy variation sequences are $\Delta_r E$= +52 kJ/mol ($\Delta_r G$= +70 kJ/mol, Reconstruction N_2) and $\Delta_r E$= +127 kJ/mol ($\Delta_r G$= -5 kJ/mol, for toluene desorption). Contrary to the methyl-cyclohexane adsorption step, these energy variations depend strongly on the order of the reconstruction/desorption steps. According to this thermodynamic analysis, we suggest that toluene desorption might preferentially occur after cluster reconstruction (as represented in **Figure 4**), although it should be confirmed by complementary activation barrier calculations.

The F → G reconstruction (with adsorbed methyl-cyclohexenyl) is exothermic and exergonic (**Table S11**). Conversely, the I → J reconstruction (with methyl-cyclohexadiene) is slightly endothermic and endergonic. The Gibbs free energies of activation for these two reconstruction steps during the reaction (F → G and I → J) are rather modest: +40 and +20 kJ/mol, respectively at 625 K. It can also be noticed that during the I → J reconstruction several H atom migrations occur simultaneously.

These structural evolutions which were first highlighted by AIMD for the adsorbed MCHe intermediate (**supporting information 3**) imply that the cluster is ductile. On purpose of quantifying more properly how the structural changes affect the energy balance, a detailed analysis of structural data and of the energy decomposition into cluster deformation, support deformation, cluster-molecule interaction, cluster-support interaction, is provided for the

adsorbed MCHe intermediate (D) in **supporting information 9**. Several insights can be learnt from the energy decomposition scheme of **Figure S12**. The first one is that the cluster structural dynamics upon 4-MCHe adsorption impacts the support-metal interaction and the intrinsic stability of the cluster itself, while the MCHe-cluster interaction is almost invariant. In particular, we find a higher stability (-96 kJ/mol) of the deformed cluster in absence of the support (after AIMD) with respect to the bilayer one. This trend is coherent with the fact that the bilayer structure is not the most stable one for non-supported Pt_{13} cluster which adopts a more three dimensional shape.[5] Simultaneously, the cluster-support interaction is significantly weakened (by more than 100 kJ/mol) for the cluster obtained after AIMD (without adsorbate). However, the crucial observation is that the cluster-support interaction is stronger after 4-MCHe adsorption than before for the deformed cluster (-13 kJ/mol), whereas it is the reverse for the reference cluster (+30 kJ/mol). Thus, the ductility reinforces the cluster-support interaction in presence of the adsorbed intermediate which counterbalances the less stable feature of the supported cluster in absence of the adsorbed intermediate after AIMD.

3.2.4 C-H bond cleavages

At 625K, the C-H dissociation steps are all exothermic and mostly exergonic except the third C-H bond cleavage from methyl-cyclohexene to methyl-cyclohexenyl+H (D → E), which is the only one to be endergonic (**Figure 7**). This step exhibits slightly positive electronic energy, the less negative enthalpy, and the largest loss of entropy (T$\Delta_r S$=-12 kJ/mol) compared to the other C-H cleavages. Additional representation of all intermediates and transition structures for these steps are shown in **Figure S13**, while their thermodynamic and kinetic features are reported in **Table S13**.
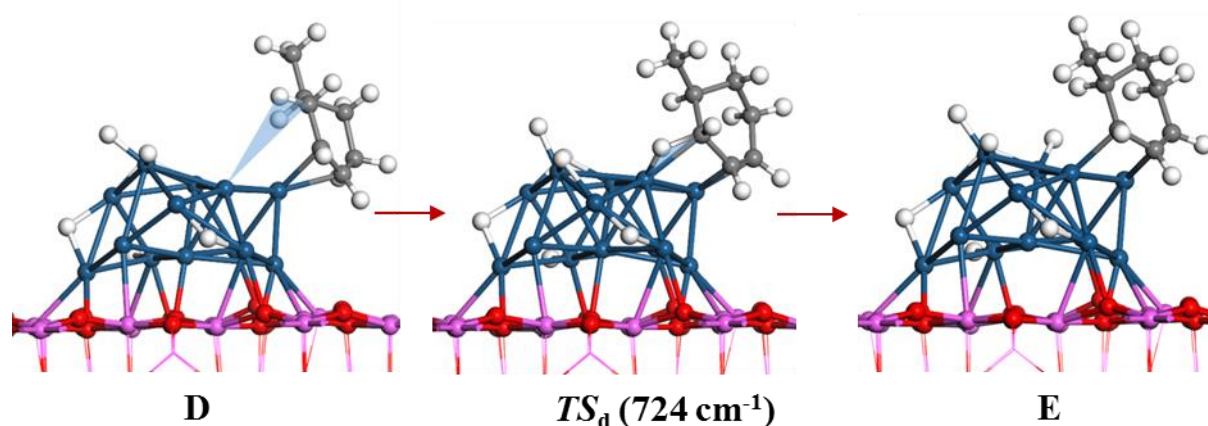
D TS_d (724 cm^{-1})   **E**

Figure 7. Molecular structure of intermediate methyl-cyclohexene (D) leading to intermediate methyl-cyclohexenyl+H (E) through the TS_d transition state. The blue triangle represents the 3 centers complex (C-H-Pt) involved during the C-H scission. The unique imaginary frequency at TS_d is given in parenthesis. Color legend: aluminum (pink balls), oxygen (red balls), platinum (dark blue balls), carbon (dark grey balls), hydrogen (white balls)

The activation free energies for the six C-H bond cleavages are comprised between +33 and +95 kJ/mol. The highest energy barrier and free energy of activation corresponds to the third C-H bond cleavage transition state (TS_d) which is coherent with the unfavorable thermodynamic data associated to this step (D→E). **Figure 7** illustrates the nature of the TS_d transition state as a 3 centers complex (C-H-Pt) which was also reported for the mono-hydrogenation steps of unsaturated alkanes on metallic surfaces.[67, 74, 78, 105, 106] It is also interesting to notice that the formation of the 3 centers complex in TS_d requires significant distortion and reorientation of the molecule from the precursor state D to the transition state TS_d as highlighted by the spatial evolution of the blue triangle (C-H-Pt) represented in **Figure 7**. Similar observations are made for the other transition states represented in **Figure S13**, which may also explain why these steps require higher activation energies.

The free energy of activation of this third C-H bond cleavage $\Delta_r G^{\ddagger}_{D \to TS_d}$ is about +95 kJ/mol with PBE-dDsC. It does not depend significantly on the functional (+103 kJ/mol with

PBE). Moreover, the three higher free energies of activation (TS_d: 95 kJ/mol, TS_l: 87 kJ/mol, TS_b: 70 kJ/mol) correspond to the three higher activation enthalpies **(Table S13)** which means that the entropic effects are moderate in these cases. The second most energy demanding step (electronic energy, enthalpy and free energy) is the last C-H bond cleavage step (TS_l) on methyl-cyclohexadienyl+H to form toluene+2H (L→M), while the third most energy demanding step corresponds to the second C-H dissociation (B→C).

Coming back to the first three steps A→B→C, it is important to underline that the energy profile strongly depends on the functional used for the calculation in this case. In line with the previous analysis of the adsorption step of MCH (A), the influence of the functional on the flat or perpendicular orientation of MCH further impacts the first C-H bond cleavage, the subsequent adsorption of methyl-cyclohexyl (B) and the second C-H bond cleavage (**Figure 8**).
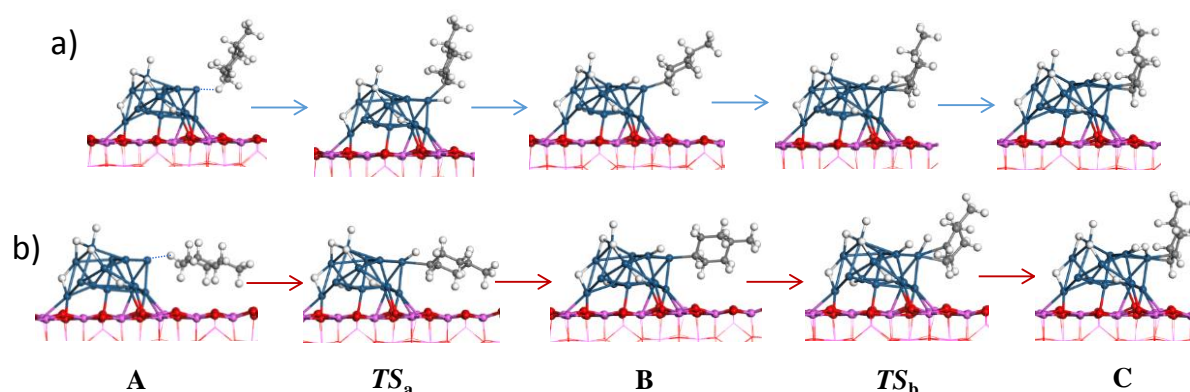

A	TS_a	B	TS_b	C

Figure 8. Comparison of the first five intermediates and transition states optimized by using a) PBE and b) PBE-dDsC functionals

As a consequence, the free energy of TS_a is increased by about 50 kJ/mol with PBE compared to the PBE-dDsC functional, which is likely due to the lack of interaction term between the molecule and the support. Moreover, the activation free energy for B → TS_b appears to be higher with PBE-dDsC ($\Delta_r G^{\ddagger}_{B \to TS_b}$ = +70 kJ/mol) than with PBE ($\Delta_r G^{\ddagger}_{B \to TS_b}$ = +52 kJ/mol). This can be explained by the fact that TS_b corresponds to a C-H bond cleavage from

intermediate B to C involving a larger rotation of the adsorbed molecule with the PBE-dDsC functional, since part of the interaction between the support and the intermediate must be broken in the transition state.

The energy values obtained for the six C-H bond cleavages steps are widespread over the intervals of 19-98 kJ/mol for reaction enthalpies and 33-95 kJ/mol for free activation energies, which enables the exploration of Brønsted−Evans−Polanyi (BEP) relationship.[107-109] Usually, such relationships aim at identifying linear correlations between the activation energy ($\Delta_r E^{\ddagger}$) and the reaction energy ($\Delta_r E$) within a given nature of elementary steps on ideal surfaces.
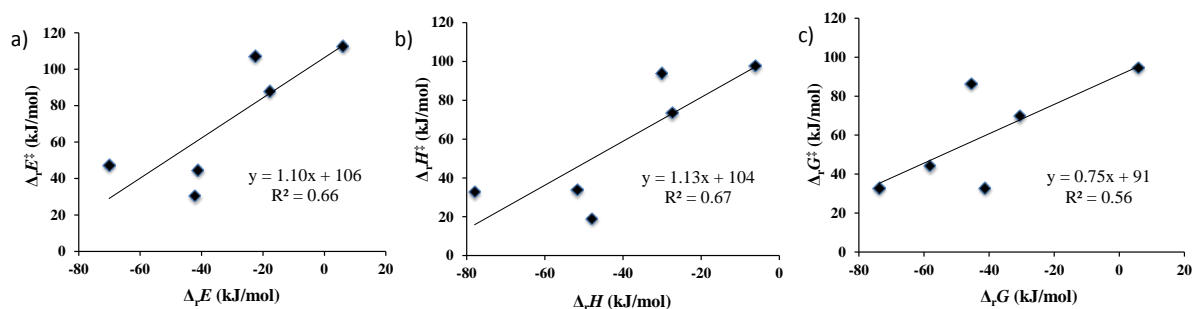

Figure 9. Brønsted−Evans−Polanyi (BEP) linear relationships based on a) electronic energy, b) enthalpy, c) free energy for C-H bond cleavage steps at PBE-dDsC level

As shown in **Figure 9**, the electronic activation energy and enthalpy exhibit a very approximate linear correlation with similar slopes, although the regression coefficient remains lower (R^2=0.66-0.67) than the ones usually reported on ideal surface. In fact, we distinguish two main families of transition states: the first one corresponding to the three highest activation energies TS_d, TS_l, and TS_b, and second one to the three lowest energies TS_a, TS_g, and TS_j. Considering the Gibbs free energy, the quality of the correlation becomes worse (R^2=0.56), which is related to supplementary entropy effects making more complicated the preservation of the linear trends.

As a consequence, contrasting with published results on ideal surfaces, enthalpy as well as free energy of activation hardly follow the expected BEP relationships because even if

they involved the breaking of similar C-H bonds, each C-H bond scission is taking place on reconstructed clusters (so with different environments of sites including H atoms vicinity): so, this structural ductility of sites screens the BEP relationships (if they exist). Moreover, the strong reorientations of the adsorbed intermediates during the C-H scission (as mentioned before) also questions the energetic link between reactant, TS, and product. This last parameter is also suspected to depend on the dispersion interaction and the entropic in the course of the elementary step. For this reason, it is interesting to underline that we find BEP relationships with improved regression coefficients (R^2=0.74-0.86) when the PBE functional is used (**Figure S14**). In particular, it appears that among the outlying data of the free energy BEP relationship (PBE-dDsC level), the first C-H bond cleavage step and the last C-H bond cleavage are concerned. Regarding the first one, it should be recalled that the MCH molecule interacts with the support in a flat configuration (**Figure 5 b**) which significantly modifies the expected chemical trends based on a pure metallic phase. With the PBE functional, the MCH molecule does not interact with the support, which may thus explain the improved BEP relationship.

4. DISCUSSION

Table 2 summarizes the various key elementary steps and their energetic values determined within this work. It appears that the C-H bond cleavage steps are the more free energy demanding steps with free energy of activation reaching 95 kJ/mol.

If we attempt to make the bridge with experimental kinetic studies, considering the three rather close higher free energies of activation, a first kinetic analysis based on a global energetic span model,[110] shows that the TOF-determining transition state (TDTS) and the TOF-determining intermediate (TDI) would be TS_d (**Table 2**) and M (toluene+2H) respectively, leading to an apparent free energy of activation of about 211 kJ/mol at 625 K.

However, this absolute value is difficult to compare directly with the apparent activation energy reported in experimental works[28, 35, 53, 55, 56, 61, 62] ranging from 15 kJ/mol up to 220 kJ/mol due also to the contribution of pre-exponential factors depending on numerous experimental parameters. If we consider instead the apparent enthalpy of activation corresponding to the previous TDTS and TDI analysis, the calculated value (382 kJ/mol) is far off the experimental one.

Table 2. Free energies of reaction and activation (in kJ/mol) for the elementary steps identified along the reaction pathway at 625 K. The second column corresponds to the highest free energy of the less stable transition state for each type of elementary step.

Elementary steps	$\Delta_r G$ or $\Delta_r G^{\ddagger}$	Highest free energy
MCH adsorption	51	51
C-H cleavage	[33 – 95]	102 (TS_d 3rd CH) - TDTS
H diffusion	[41 – 42]	54 (TS_e)
Cluster reconstruction	[20 – 40]	50 (TS_f)
H$_2$ desorption	[29 – 65]	7 (1st H$_2$ des.)
Toluene desorption	44	44

The energetic span analysis further reveals that the apparent free energy of activation depends on the energy level of TS_d and M which means that the TS of the third C-H bond cleavage would be a critical state as well as the thermodynamic stability of (toluene+2H) adsorbed on the cluster. It also shows that the TDTS is difficult to be identified unambiguously considering the DFT accuracy as TS_a and TS_b free energies are rather close to TS_d. In particular, at higher temperature 800K, these TS_a and TS_b states may become TDTS (**Table S6**) due to entropic effects which destabilize most of the initial part of the dehydrogenation pathway, whereas TS_d is rather insensitive to temperature effect. This may also explain the difficulty for experimentalist to identify unambiguously the rate limiting steps.

In particular, Alhumaidan et al.[56] and Usman et al.[55] studied the kinetics of methylcyclohexane of dehydrogenation on a Pt(1.0 wt%)/γ-Al$_2$O$_3$ catalyst. They used a non-

competitive Horiuti-Polanyi mechanism based on the 6 successive C-H bond cleavages which may be comparable to our current DFT model, although they do not explicitly consider any cluster reconstruction steps and H migration steps. They proposed that the first MCH mono-dehydrogenation step is the rate limiting step as it was also early suggested by others.[62, 111] This approach leads to an activation energy of 55.4[56] and 50.9[55] kJ/mol for this step in a temperature range of 613-653 K. Usman et al.[55] also performed a single site LHHW model, and proposed that the dehydrogenation of adsorbed MCH leading to adsorbed MCHe and one gaseous hydrogen molecule is the rate-determining step, with an activation energy of 39.3 kJ/mol (without entropy contribution). This value is consistent with our calculated activation energy (+31 kJ/mol), considering cumulative steps A→D as in the Usman's model. However, this low value indicates that the first MCH dehydrogenation step alone is not rate limiting according to our DFT analysis. When coupling the MCH adsorption with the first MCH mono-dehydrogenation step, the integrated free energy of activation becomes +84 kJ/mol at 625 K, which falls within a similar range as the three highest calculated free energies of activation of C-H bond cleavages.

Other authors[35, 54, 112] suggest that the rate limiting step is not the first MCH dehydrogenation but rather a subsequent step involving unsaturated intermediates. Van Trimpont et al.[35] studied various single and dual site models within a LHHW mechanism for MCH dehydrogenation on sulfided Pt (0.59 wt.%) /γ-Al$_2$O$_3$ catalyst at T=643 K. Among these various possible models, they found that the rate-determining steps would involve the following unsaturated intermediates : methylcyclohexene → methyl-cyclohexadiene (with activation enthalpy of +57 kJ/mol), methyl-cyclohexadiene → toluene (+76 kJ/mol), methyl-cyclohexenyl → methyl-cyclohexadiene (G → H, 68 kJ/mol) or methyl-cyclohexadienyl → toluene (L → M, +91 kJ/mol). These values are consistent with our DFT values of activation

enthalpies which are comprised between +33 and +95 kJ/mol for the corresponding monohydrogenation steps (**Table 2**).

From a more general point of view, we cannot exclude that the cluster's ductility may also be at the origin of the encountered difficulties to find in the experimental literature a general consensus on the kinetic parameters of this important reaction. Indeed, the cluster reconstruction is suspected to depend on subtle changes in reaction conditions (temperature but also partial pressure of reactants and hydrogen)[1, 7] and also on the nature of the support (hydrated state, morphology).[6] So, the kinetic results might depend on the initial surface state of the experimental system. As we underlined it in introduction, it is still questioned whether the MCH dehydrogenation is a structure-sensitive or insensitive reaction particularly in the case of highly dispersed metallic particles.[20-28, 113] Contrasting with the earlier Boudart's classification,[20] Rioux et al. found that cyclohexene dehydrogenation would be size sensitive in the case of Pt nanoparticles supported on SBA-15.[28] Moreover, Rochefort et al. suggested that instead of a true size sensitivity, the methylcyclohexane dehydrogenation is sensitive to the platinum cluster structure when supported on alumina.[26] Considering the present DFT results, we showed that thanks to its ductility, the Pt cluster adapts its nano-structure in order to minimize the free energy profile. In essence, the dehydrogenation reaction is thus sensitive to the sites' structure as proposed in [26]. Nevertheless, since the cluster sites' structure evolve in the course of the reaction, it happens to be very difficult for experimentalists to identify if such a structure sensitivity relationship holds for supported sub-nanometric metallic particles. According to previous theoretical works, [8, 9] this observation can certainly be generalized to other reactions catalyzed by sub-nanometric metallic particles whose the ductile character of the metal is involved.

Another important aspect concerns the impact of H and HC coverages of the Pt_{13} cluster. As mentioned previously, our initial choice on H coverage results from a compromise

between previous DFT calculations[7] and in situ XANES observations[1]. In our previous work[8] the ratio of partial pressure $P(H_2)/P(HC)$ was also considered as a relevant parameter for the system. Usually, for the naphtha reforming conditions, the $P(H_2)/P(HC)$ is higher than 4 with a $P(H_2)$ value comprised between 20-30 bars in the case of a pure Pt cluster. So the chosen configuration is probably an optimal value of intermediate H coverage for the targeted reaction. If we assume that less H atoms are present on the cluster, the energy required to desorb the dissociated H atoms will perhaps become a limiting step. If the cluster's coverage by HC simultaneously increases, this would probably lead to strong steric constraints between HC molecules reducing their approaches to Pt sites. If on the contrary, we consider that more H atoms are present on the cluster, this will progressively disfavors the dehydrogenation steps by blocking the Pt sites required for C-H dehydrogenation. This qualitative analysis means that experimental kinetic interpretations are suspected to strongly depend on the $P(H_2)/P(HC)$ conditions and also to the reduction pre-treatment applied to the supported Pt clusters as revealed by [113].

5. CONCLUSIONS

This work aimed at the investigation of the reactivity of metallic nano-aggregates, composed of platinum supported on γ-alumina, as models of catalytic reforming catalysts. We addressed the simulation of the dehydrogenation reaction of methyl-cyclohexane into toluene over Pt_{13} clusters supported on γ-Al_2O_3 (100) surface by using periodic density functional theory (DFT) calculations at the PBE-dDsC and PBE levels in combination with first principles molecular dynamics approach.

From a methodological point of view, the dispersion corrections as implemented in the PBE-dDsC functional not only lower the free energy profile, but also modify the adsorption configuration of the first two intermediates. The physisorbed methyl-cyclohexane and

chemisorbed methyl-cyclohexyl are both stabilized by a dual interaction with the alumina surface and the cluster, which is only described with the PBE-dDsC functional. We also show the paramount importance of the quantification of free energies of activation to recover the temperature effect mainly related to entropy, which mostly affects the adsorption/desorption steps of methyl-cyclohexane, H_2 and toluene respectively.

In addition to these adsorption and desorption steps, we found that the optimal reaction pathway consists of six subsequent C-H bond cleavages combined to H diffusion and/or cluster reconstruction steps. Our results show that many elementary steps are competing. At 625 K, the highest activation free energy found corresponds to the third C-H cleavage step (TS_d) of methyl-cyclohexene into methyl-cyclohexenyl + H, with a free activation energy of +95 kJ/mol at the PBE-dDsC level. However, the free activation energies of several other steps are competitive, as a function of the temperature, such as the second or last C-H cleavage step. Moreover, we cannot exclude that the toluene desorption step coupled to the desorption of the last H_2 molecule may become rate limiting. The first C-H bond cleavage often invoked as the rate limiting step, is only so if we integrate it with the MCH adsorption step. This trend also explains why kinetic parameters reported in the literature fluctuate significantly from one experimental study to another.

As a first perspective, we hope that the DFT data provided in the present work will help for establishing a coherent ab initio microkinetic model to provide a more robust interpretation of kinetic experimental data on the basis of rate constants calculated with activation energies determined here. Such a modeling approach, from elementary steps studied ab initio to the calculation of macroscopic data, should allow the comparison with the conventional kinetic fitting modeling approaches discussed in the present work. However, according to the present finding the definition of the site must be revisited in such kinetic modeling, and the conventional Langmuir-Hinshelwood formalism cannot be

straightforwardly applied due to the active site reconstruction which should be considered itself as an elementary step.

Moreover, none of the current experimental studies invoked the possible role of structural evolution (so called ductility effect) of the supported Pt cluster during the reaction. To enable the occurrence of these C-H bond cleavage steps at the core of the dehydrogenation reaction, we found that the catalytic system is ductile and must reorganize the Pt cluster atomic structure to make the active site optimal for C-H bond cleavage. Simultaneously, this cluster ductility induces also hydrogen atom migration on the cluster. To describe properly this major effect, molecular dynamics simulation was mandatory to explore the alternative cluster structures and hydrogen position. This cluster ductility together with fluctuation of dispersion interactions also explain why the BEP linear relationship related to C-H cleavage steps exhibit a rather poor correlation coefficient. At this stage, we must acknowledge that molecular dynamics approaches would also be highly profitable to the refinement of the reaction pathway. In particular, biased molecular dynamics would capture even more accurately the evolution of the cluster conformation during each elementary step and probably smooth the whole free energy profile. However, it is likely that that the main finding on the effect of cluster ductility would even be enhanced.

A final important consequence concerns the historical "structure sensitivity/insensitivity" concept invoked in catalysis.[20] This cluster shape change in the course of a reaction makes more difficult to identify if a reaction (such as the dehydrogenation) is structure-sensitive or insensitive particularly in the case of supported metallic particles.[26] Indeed, since the structure of highly dispersed metallic particles are themselves sensitive to the reaction conditions, the concept of structure sensitivity of the reaction is scrambled by the ductility of the cluster.

REFERENCES

[1] A. Gorczyca, V. Moizan, C. Chizallet, O. Proux, W. Del Net, E. Lahera, J.L. Hazemann, P. Raybaud, Y. Joly, Angew. Chem. Int. Ed. 53 (2014) 12426.
[2] H. Mistry, F. Behafarid, S.R. Bare, B. Roldan Cuenya, ChemCatChem 6 (2014) 348.
[3] C. Jensen, D. Buck, H. Dilger, M. Bauer, F. Phillipp, E. Roduner, Chem. Commun. (Cambridge, U. K.) 49 (2013) 588.
[4] A. Halder, L.A. Curtiss, A. Fortunelli, S. Vajda, J. Chem. Phys. 148 (2018).
[5] C.H. Hu, C. Chizallet, H. Toulhoat, P. Raybaud, Phys. Rev. B 79 (2009) 195416.
[6] C.H. Hu, C. Chizallet, C. Mager-Maury, M. Corral-Valero, P. Sautet, H. Toulhoat, P. Raybaud, J. Catal. 274 (2010) 99.
[7] C. Mager-Maury, G. Bonnard, C. Chizallet, P. Sautet, P. Raybaud, ChemCatChem 3 (2011) 200.
[8] P. Raybaud, C. Chizallet, C. Mager-Maury, M. Digne, H. Toulhoat, P. Sautet, J. Catal. 308 (2013) 328.
[9] G. Sun, P. Sautet, J. Am. Chem. Soc. 140 (2018) 2812.
[10] Y.P. Chiu, L.W. Huang, C.M. Wei, C.S. Chang, T.T. Tsong, Phys. Rev. Lett. 97 (2006).
[11] H. Zhai, A.N. Alexandrova, ACS Catal. 7 (2017) 1905.
[12] E. Bus, J.A. van Bokhoven, Phys. Chem. Chem. Phys. 9 (2007) 2894.
[13] F.A. Cotton, J. Organomet. Chem. 100 (1975) 29.
[14] P.-Y. Le Goff, W. Kostka, J. Ross, Catalytic Reforming, in: Springer (Ed.) Springer Handbook of Petroleum Technology, 2017.
[15] J.H.B. Sattler, J. Ruiz-Martinez, E. Santillan-Jimenez, B.M. Weckhuysen, Chem. Rev. 114 (2014) 10613.
[16] J. Zhu, M.L. Yang, Y.D. Yu, Y.A. Zhu, Z.J. Sui, A. Holmen, D. Chen, ACS Catal. 5 (2015) 6310.
[17] P. Leprince, 3 Procédés de Transformation, Technip, 1998.
[18] T. Gjervan, R. Prestvik, A. Holmen, Basic Principles in Applied Catalysis, Springer, 2004.
[19] M.R. Rahimpour, M. Jafari, D. Iranshahi, Appl. Energy 109 (2013) 79.
[20] M. Boudart, Adv. Catal. 20 (1969) 153.
[21] J.A. Cusumano, G.W. Dembinski, J.H. Sinfelt, J. Catal. 5 (1966) 471.
[22] J.H. Sinfelt, Catalytic Reforming, in: in: G. Ertl, E. Knözinger, J. Weitkamp (Eds.), Handbook of Heterogeneous Catalysis, Wiley, Weinheim, pp. 1939.
[23] J.H. Sinfelt, Bifunctional Catalysis, in Advances in Chemical Engineering, Academic Press, 1964.
[24] M. Guenin, M. Breysse, R. Frety, K. Tifouti, P. Marecot, J. Barbier, J. Catal. 105 (1987) 144.
[25] R.K. Herz, W.D. Gillespie, E.E. Petersen, G.A. Somorjai, J. Catal. 67 (1981) 371.
[26] A. Rochefort, F. Le Peltier, J.P. Boitiaux, J. Catal. 145 (1994) 409.
[27] G.A. Somorjai, J.Y. Park, Chem. Soc. Rev. 37 (2008) 2155.
[28] R.M. Rioux, B.B. Hsu, M.E. Grass, H. Song, G.A. Somorjai, Catal. Lett. 126 (2008) 10.
[29] R.A. Van Santen, Acc. Chem. Res. 42 (2009) 57.

[30] D.M. Little, Catalytic Reforming, Pennwell Publ Co. , Oklahoma, 1985.

[31] A.N. Jahel, V. Moizan-Baslé, C. Chizallet, P. Raybaud, J. Olivier-Fourcade, J.C. Jumas, P. Avenier, S. Lacombe, J. Phys. Chem. C 116 (2012) 10073.

[32] A. Jahel, P. Avenier, S. Lacombe, J. Olivier-Fourcade, J.C. Jumas, J. Catal. 272 (2010) 275.

[33] F. Ahmed, M.K. Alam, A. Suzuki, M. Koyama, H. Tsuboi, N. Hatakeyama, A. Miyamoto, J. Phys. Chem. C 113 (2009) 15676.

[34] K. Jothimurugesan, A.K. Nayak, G.K. Mehta, K.N. Rai, S. Bhatia, R.D. Srivastava, AIChE J. 31 (1985) 1997.

[35] P.A. Van Trimpont, G.B. Marin, G.F. Froment, Ind. Eng. Chem. Fundam. 25 (1986) 544.

[36] J.L. Carter, G.B. McVicker, W. Wissman, W.S. Kmak, J.H. Sinfelt, Appl. Catal. 3 (1982) 327.

[37] A.S. Fung, M.J. Kelley, D.C. Koningsberger, B.C. Gates, J. Am. Chem. Soc. 119 (1997) 5877.

[38] J.M. Parera, J.N. Beltramini, C.A. Querini, E.E. Martinelli, E.J. Churin, P.E. Aloe, N.S. Figoli, J. Catal. 99 (1986) 39.

[39] A.C. Muller, J. Catal. 72 (1979) 65.

[40] R. Burch, L. Garla, J. Catal. 71 (1981) 360.

[41] R. Srinivasan, B.H. Davis, Platinum Metals Rev. 36 (1991) 151.

[42] G.J. Siri, G.R. Bertolini, M.L. Casella, O.A. Ferretti, Mater. Lett. 59 (2005) 2319.

[43] N. Macleod, J.R. Fryer, D. Stirling, G. Webb, Catal. Today 46 (1998) 37.

[44] B.H. Davis, Catal. Today 53 (1999) 443.

[45] N.S. Figoli, M.R. Sad, J.N. Beltramini, E.L. Jabioski, J.M. Parera, Ind. Eng. Chem. Prod. Res. Dev 19 (1980) 545.

[46] M. Digne, P. Raybaud, P. Sautet, D. Guillaume, H. Toulhoat, J. Am. Chem. Soc. 130 (2008) 11030.

[47] C.G. Myers, W.H. Lang, P.B. Weisz, Ind. Eng. Chem. Res. 53 (1961) 299.

[48] J. Beltramini, D.L. Trimm, Appl. Catal. 31 (1987) 113.

[49] J.H. Sinfelt, J. Mol. Catal. A: Chem. 163 (2000) 123.

[50] G.C. Bond, R.H. Cunningham, J. Catal. 166 (1997) 172.

[51] X. Liu, W.Z. Lang, L.L. Long, C.L. Hu, L.F. Chu, Y.J. Guo, Chem. Eng. J. (Lausanne) 247 (2014) 183.

[52] A. Touzani, D. Klvana, G. Belanger, Studies Surf. Sci. Catal. - Catalysis on the Energy Scene 19 (1984) 357.

[53] H.J. Sinfelt, H. Hurwitz, R.A. Shulman, J. Phys. Chem. 64 (1960) 1559.

[54] J. Verstraete, Kinetische Studie van de Katalytische Reforming van Nafta over een Pt-Sn/Al2O3 Katalysator - PhD Thesis, in, Universiteit Gent, 1997.

[55] M. Usman, D. Cresswell, A. Garforth, Ind. Eng. Chem. Res. 51 (2012) 158.

[56] F. Alhumaidan, D. Cresswell, A. Garforth, Ind. Eng. Chem. Res. 50 (2011) 2509.

[57] M. Boudart, AIChE J. 2 (1956) 62.

[58] E.E. Wolf, E.E. Petersen, J. Catal. 46 (1977) 190.

[59] J.F.G. Delabanda, A. Corma, F.V. Melo, Appl. Catal. 26 (1986) 103.

[60] M.A. Rodríguez, J. Ancheyta, Fuel 90 (2011) 3492.

[61] G. Maria, A. Marin, C. Wyss, S. Muller, E. Newson, Chem. Eng. Sci. 51 (1996) 2891.

[62] A. Touzani, D. Klvana, G. Belanger, Stud. Surf. Sci. Catal. 19 (1984) 357.

[63] C. Chizallet, P. Raybaud, Catal. Sci. Technol. 4 (2014) 2797.

[64] C. Mager-Maury, C. Chizallet, P. Sautet, P. Raybaud, ACS Catal. 2 (2012) 1346.

[65] H. Steininger, H. Ibach, S. Lehwald, Surf. Sci. 117 (1982) 685.

[66] Y. Chen, D.G. Vlachos, J. Phys. Chem. C 114 (2010) 4973.

[67] M. Neurock, R.A. van Santen, J. Phys. Chem. B 104 (2000) 11127.

[68] H.A. Aleksandrov, L.V. Moskaleva, Z.J. Zhao, D. Basaran, Z.X. Chen, D.H. Mei, N. Rösch, J. Catal. 285 (2012) 187.
[69] C. Breinlich, J. Haubrich, C. Becker, A. Valcarcel, F. Delbecq, K. Wandelt, J. Catal. 251 (2007) 123.
[70] S. Saerens, M.K. Sabbe, V.V. Galvita, E.A. Redekop, M.F. Reyniers, G.B. Marin, ACS Catal. 7 (2017) 7495.
[71] C. Morin, D. Simon, P. Sautet, J. Phys. Chem. B 108 (2004) 5653.
[72] C. Morin, D. Simon, P. Sautet, J. Phys. Chem. B 108 (2004) 12084.
[73] C. Morin, D. Simon, P. Sautet, Surf. Sci. 600 (2006) 1339.
[74] M. Saeys, M. Reyniers, J. Thybaut, M. Neurock, G.B. Marin, J. Phys. Chem. B 109 (2005) 2064.
[75] M. Saeys, M. Reyniers, J. Thybaut, M. Neurock, G.B. Marin, J. Catal. 236 (2005) 129.
[76] G. Canduela-Rodriguez, M.K. Sabbe, M.F. Reyniers, J.F. Joly, G.B. Marin, Phys. Chem. Chem. Phys. 16 (2014) 23754.
[77] M.K. Sabbe, G. Canduela-Rodriguez, M.F. Reyniers, G.B. Marin, J. Catal. 330 (2015) 406.
[78] H.Y. Ma, G.C. Wang, J. Catal. 281 (2011) 63.
[79] M. Digne, P. Sautet, P. Raybaud, P. Euzen, H. Toulhoat, J. Catal. 226 (2004) 54.
[80] M. Digne, P. Sautet, P. Raybaud, P. Euzen, H. Toulhoat, J. Catal. 211 (2002) 1.
[81] X. Krokidis, P. Raybaud, A.E. Gobichon, B. Rebours, P. Euzen, H. Toulhoat, J. Phys. Chem. B 105 (2001) 5121.
[82] G. Kresse, F. J., Comput. Mater. Sci. 6 (1996) 15.
[83] G. Kresse, J. Furthmüller, Phys. Rev. B: Condens. Matter Mater. Phys. 54 (1996) 11169.
[84] J.P. Perdew, B. Kieron, M. Ernzerhof, Phys. Rev. Lett. 77 (1996) 3865.
[85] S.N. Steinmann, C. Corminboeuf, J. Chem. Theory Comput. 7 (2011) 3567.
[86] S.N. Steinmann, C. Corminboeuf, J. Chem. Phys. 134 (2011) 044117.
[87] S. Gautier, S.N. Steinmann, C. Michel, P. Fleurat-Lessard, P. Sautet, Phys. Chem. Chem. Phys. 17 (2015) 28921.
[88] P.E. Blöchl, Phys. Rev. B 50 (1994) 17953.
[89] G. Kresse, J. Joubert, Phys. Rev. B 59 (1999) 1758.
[90] B. Wang, G.F. Froment, Catal. Lett. 147 (2017) 663.
[91] P.A. Van Trimpont, G.B. Marin, G.F. Froment, Appl. Catal. 17 (1985) 161.
[92] F.C. Henn, A.L. Diaz, M.E. Bussell, M.B. Hugenschmidt, M.E. Domagala, C.T. Campbell, J. Phys. Chem. B 96 (1992) 5965.
[93] O. Lytken, W. Lew, C.T. Campbell, Chem. Soc. Rev. 37 (2008) 2172.
[94] G. Henkelman, H. Jónsson, J. Chem. Phys. 113 (2000) 9978.
[95] D. Sheppard, R. Terrell, G. Henkelman, J. Chem. Phys. 128 (2008).
[96] P. Fleurat-Lessard, Opt'n Path, in: http://pfleurat.free.fr/ReactionPath.php.
[97] http://theory.cm.utexas.edu/vtsttools/, in.
[98] G. Henkelman, B.P. Uberuaga, H. Jonsson, J. Chem. Phys. 113 (2000) 9901.
[99] P. Pulay, Chem. Phys. Lett. 73 (1980) 393.
[100] J.M. Tonnerre, D. Raoux, J.C.d. Lima, H. Toulhoat, D. Espinat, J. Phys. C9 (1987) 1137.
[101] F. Mittendorfer, C. Thomazeau, P. Raybaud, H. Toulhoat, J. Phys. Chem. B 107 (2003) 12287.
[102] S. Gautier, P. Sautet, J. Phys. Chem. C 121 (2017) 25152.
[103] N.B. Arboleda, H. Kasai, W.A. Dino, H. Nakanishi, Japanese Journal of Applied Physics Part 1-Regular Papers Brief Communications & Review Papers 46 (2007) 4233.
[104] R.A. Olsen, G.J. Kroes, E.J. Baerends, J. Chem. Phys. 111 (1999) 11155.
[105] F. Delbecq, D. Loffreda, P. Sautet, J. Phys. Chem. Lett. 1 (2010) 323.

[106] S. Vajda, M.J. Pellin, J.P. Greeley, C.L. Marshall, L.A. Curtiss, G.A. Ballentine, J.W. Elam, S. Catillon-Mucherie, P.C. Redfern, F. Mehmood, P. Zapol, Nat. Mater. 8 (2009) 213.
[107] R.P. Bell, Proc. R. Soc. London 154 (1936) 414.
[108] M.G. Evans, M. Polanyi, Trans. Faraday Soc. 33 (1937) 448.
[109] M.G. Evans, M. Polanyi, Trans. Faraday Soc. 34 (1938) 11.
[110] S. Kozuch, S. Shaik, Acc. Chem. Res. 44 (2011) 101.
[111] J. Chaouki, A. Touzani, D. Klvana, J.P. Bournonville, G. Belanger, Revue De L'Institut Francais Du Pétrole 43 (1988) 873.
[112] R.W. Maatman, P. Mahaffy, P. Hoekstra, C. Addink, J. Catal. 23 (1971) 105.
[113] A. Rochefort, F. Lepeltier, J.P. Boitiaux, J. Catal. 138 (1992) 482.